



**HAL**  
open science

## Effects of cobalt doping on the reactivity of hausmannite for As(III) oxidation and As(V) adsorption

Shuang Zhang, Hui Li, Zhongkuan Wu, Jeffrey Post, Bruno Lanson, Yurong Liu, Biyun Hu, Mingxia Wang, Limei Zhang, Mei Hong, et al.

### ► To cite this version:

Shuang Zhang, Hui Li, Zhongkuan Wu, Jeffrey Post, Bruno Lanson, et al.. Effects of cobalt doping on the reactivity of hausmannite for As(III) oxidation and As(V) adsorption. *Journal of Environmental Sciences*, 2022, 122, pp.217-226. 10.1016/j.jes.2022.02.004 . insu-03833487

**HAL Id: insu-03833487**

**<https://insu.hal.science/insu-03833487>**

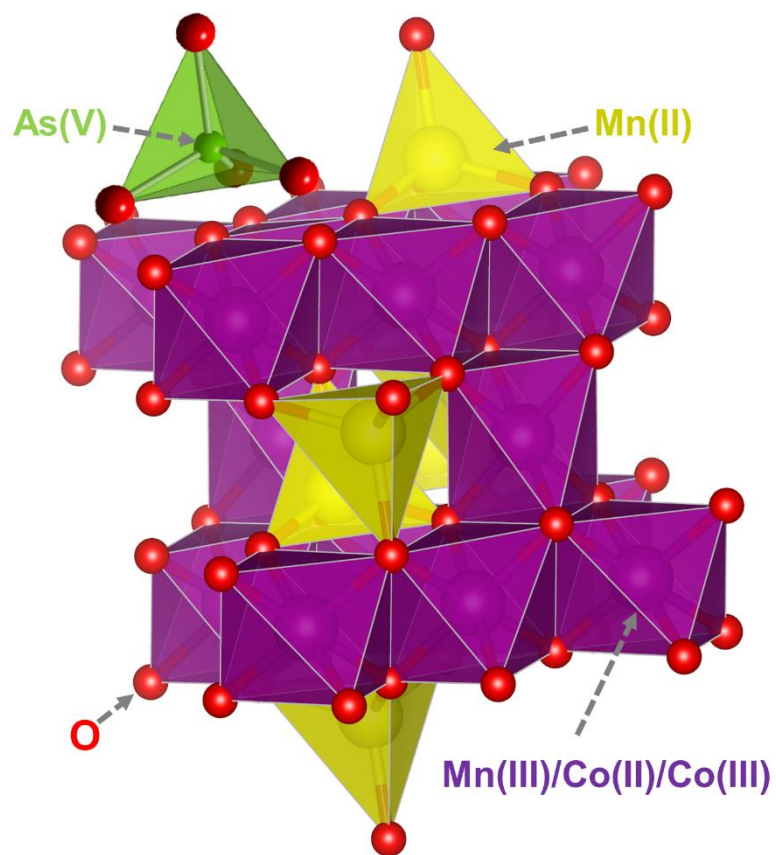
Submitted on 28 Oct 2022

**HAL** is a multi-disciplinary open access archive for the deposit and dissemination of scientific research documents, whether they are published or not. The documents may come from teaching and research institutions in France or abroad, or from public or private research centers.

L'archive ouverte pluridisciplinaire **HAL**, est destinée au dépôt et à la diffusion de documents scientifiques de niveau recherche, publiés ou non, émanant des établissements d'enseignement et de recherche français ou étrangers, des laboratoires publics ou privés.



**Graphical Abstract:**



28

29

30 **Abstract:** Hausmannite is a common low valence Mn oxide mineral, with a distorted  
31 spinel structure, in surficial sediments. Although natural Mn oxides often contain  
32 various impurities of transitional metals (TMs), few studies have addressed the effect  
33 and related mechanism of TM doping on the reactivity of hausmannite with metal  
34 pollutants. Here, the reactivity of cobalt (Co) doped hausmannite with aqueous As(III)  
35 and As(V) was studied. Co doping decreased the point of zero charge of hausmannite  
36 and its adsorption capacity for As(V). Despite a reduction of the initial As(III) oxidation  
37 rate, Co-doped hausmannite could effectively oxidize As(III) to As(V), followed by the  
38 adsorption and fixation of a large amount of As(V) on the mineral surface. Arsenic K-  
39 edge EXAFS analysis of the samples after As(V) adsorption and As(III) oxidation  
40 revealed that only As(V) was adsorbed on the mineral surface, with an average As-Mn  
41 distance of 3.25–3.30 Å, indicating the formation of bidentate binuclear complexes.  
42 These results provide new insights into the interaction mechanism between TMs and  
43 low valence Mn oxides and their effect on the geochemical behaviors of metal  
44 pollutants.

45 **Keywords:** Mn oxide; hausmannite; transition-metal; cobalt; arsenate adsorption;  
46 arsenite oxidation.

47

48

49

50

51

52

53

54

55

56

57

58

## 59 **Introduction**

60 Hausmannite, the fifth most common Mn oxide mineral in soils and sediments, is  
61 commonly present in hydrothermal and metamorphic deposits (Giovannelli et al., 2012;  
62 Peña et al., 2007). It has considerable adsorption and redox reactivity for a variety of  
63 metal pollutants (Barreto et al., 2020; Shaughnessy et al., 2003; Song et al., 2020; Wilk  
64 et al., 2005). Compared with other Mn oxides, hausmannite has a high point of zero  
65 charge (Barreto et al., 2020; Shaughnessy et al., 2003), and thus may carry a positive  
66 charge even under near-neutral pH conditions, which may greatly promote its  
67 adsorption reactivity with anionic pollutants such as arsenate ( $\text{As(V)O}_4^{3-}$ ). Arsenate  
68 pollution has aroused great environmental concerns globally due to its high toxicity  
69 (Choong et al., 2007; Habuda-Stanic and Nujic, 2015). Adsorption by minerals such as  
70 hausmannite has been demonstrated to be an effective way to remove As(V) from  
71 wastewaters. Previous studies have shown that the adsorption capacity of hausmannite  
72 for As(V) gradually decreases with increasing pH (Barreto et al., 2020; Garcia et al.,  
73 2014). However, there have also been some reports about the pH-independent  
74 adsorption of hausmannite for As(V) (Parsons et al., 2009). The various coexisting  
75 anions ( $\text{SO}_4^{2-}$ ,  $\text{PO}_4^{3-}$ ,  $\text{Cl}^-$  and  $\text{NO}_3^-$ ) have minor effects on As(V) adsorption (Garcia et  
76 al., 2014).

77 Hausmannite can also oxidize low-valence redox-sensitive elements such as As(III)  
78 and Cr(III) (Garcia et al., 2014; Weaver and Hochella Jr., 2003; Xu et al., 2017). It has  
79 been added to paddy soils to enhance arsenite oxidation and retention, thereby reducing  
80 the mobility and toxicity of soil As (Xu et al., 2017). The oxidation of As(III) by  
81 hausmannite is greatly affected by the reaction pH. It has been reported that the  
82 oxidation of As(III) is significantly more efficient with increasing pH from 7 to 12  
83 (Feng et al., 2006). Under acidic conditions, the maximum binding of As(III) on  
84 hausmannite was observed at pH 4–5 (Feng et al., 2006; Parsons et al., 2009); however,

85 a reduction of As(III) adsorption with increasing pH from 2 to 6 was also reported  
86 (Garcia et al., 2014). Ionic strength (e.g., Cl<sup>-</sup>) has little influence on As(III) adsorption  
87 (Feng et al., 2006). Low concentrations of tartaric acid promotes the oxidation of  
88 As(III), but tartaric acid at high concentrations inhibits the reaction (Feng et al., 2006).  
89 After As(III) oxidation, the changes in the average hausmannite particle sizes were  
90 minimal and could not be detected by XRD analysis (Parsons et al., 2009). In a previous  
91 study, As K-edge XANES analysis for the reaction of hausmannite and hausmannite-  
92 magnetite with As(III) at an initial pH of 5 and a final pH of 6–7 demonstrated that all  
93 As retained on the mineral surface was As(V) (Silva et al., 2012). Raman and FTIR  
94 analysis revealed that As(V) was adsorbed on these minerals as monodentate  
95 mononuclear (MM) and bidentate mononuclear (BM) complexes (Silva et al., 2013).  
96 Recently, investigation of As(V) adsorption onto hausmannite using attenuated total  
97 reflection-Fourier transform infrared (ATR-FTIR) spectroscopy demonstrated that  
98 As(V) was adsorbed onto hausmannite surfaces as bidentate complexes at high pH  
99 during the early adsorption stage and with low surface coverage. With decreases in pH  
100 and increases in adsorption time and surface loading, more As(V) species were  
101 adsorbed as outer-sphere and/or protonated inner-sphere monodentate species (Barreto  
102 et al., 2020). As K-edge extended X-ray absorption fine structure (EXAFS)  
103 spectroscopy demonstrated that As adsorbed on hausmannite surfaces through As(V)  
104 adsorption and As(III) oxidation at pH 5 formed binuclear bidentate complexes  
105 (Parsons et al., 2009).

106 Mn oxide minerals in various geological settings are often enriched in various  
107 transition metals (TMs) (Baron et al., 1998). Incorporation of TMs into Mn oxides can  
108 modify their structure, physicochemical properties and reactivities with various  
109 pollutants (Song et al., 2020; Yin et al., 2012). Our previous studies investigated the  
110 effects of TMs on the reactivity of hexagonal birnessite with various pollutants. The  
111 results clearly demonstrated that TM-containing minerals, which are closer to natural  
112 analogs, tend to have much different reactivities with pollutants compared with the  
113 corresponding pristine minerals. For example, incorporation of Ni into hexagonal

114 birnessite greatly reduced the adsorption capacity of birnessite for heavy metals (Pb(II)  
115 or Zn(II)) by 79%–85% (Yin et al., 2012). The removal efficiencies of Cr(III) from  
116 water by Co- and Ni-containing birnessite were only 28%–55% and 67%–78% that of  
117 pure birnessite, respectively (Yin et al., 2020). As a low-valence Mn oxide, hausmannite  
118 is also capable of incorporating various substituents including Co, Ni, Fe and Al (Antao  
119 et al., 2019; Baron et al., 1998; Bordeneuve et al., 2010; Song et al., 2020). Substitution  
120 of Fe(III) for Mn(III) into the octahedral site of hausmannite decreases the Jahn-Teller  
121 distortion, increases the Curie point, and decreases the spontaneous magnetization  
122 (Baron et al., 1998). Zn doping changes the morphology of hausmannite crystallites  
123 from nanorods to a mixture of nanorods and nanoparticles, as well as increases the  
124 energy band gap (Jha et al., 2012). Pb doping greatly reduces the Mn<sub>3</sub>O<sub>4</sub> particle size  
125 and increases the energy band gap, dielectric constant, and AC conductivity (Şahin et  
126 al., 2020). Doping with various TMs (Cr(III), Co(II), Ni(II), and Cu(II)) can greatly  
127 enhance the phase stability during cycling and charge-transfer behaviors of  
128 hausmannite (Dong et al., 2013). However, these studies were mainly focused on the  
129 application of TM-modified hausmannite in material sciences, and few studies have  
130 been carried out to explore the dopant effects on the reactivity of hausmannite with  
131 environmental pollutants. It has been recently reported that Ni substitution in  
132 hausmannite leads to noticeable changes in the mineral structure (e.g. lattice  
133 parameters), and enhances the acid dissolution and oxidation reactivity of hausmannite  
134 with As(III) at pH 5 (Song et al., 2020). These findings indicate that impurities may  
135 modify the structure and physicochemical properties of hausmannite and thus alter its  
136 adsorption behavior and redox reactivity with pollutants. Unlike Ni, Co is highly redox-  
137 sensitive, and the influence of Co incorporation on the reactivity and stability of  
138 hausmannite remains to be elucidated.

139 In this study, we investigated the effect of Co doping on the reactivity of  
140 hausmannite for the removal of As(III) and As(V) from water. The influence of  
141 environmental conditions (pH and ionic strength) on the As(V) adsorption by Co-doped  
142 hausmannite was also studied. For As(III) oxidation, changes in the concentration of

143 various As species were also monitored during oxidation. As K-edge EXAFS data from  
144 samples after both As(V) adsorption and As(III) oxidation were collected and analyzed  
145 to reveal the adsorption mechanisms. Our results provide new insights into the  
146 interaction mechanisms of low valence Mn oxides with TMs, and the influences of  
147 these minerals on the geochemical behaviors of heavy metal pollutants in surficial  
148 environments.

## 149 **1 Materials and methods**

### 150 **1.1 Chemical and materials**

151 All chemical reagents used in this study were purchased from Sinopharm  
152 Chemical Reagent Co. Ltd., China. Manganese sulfate ( $\text{MnSO}_4 \cdot \text{H}_2\text{O}$ ; analytical grade),  
153 cobalt sulfate ( $\text{CoSO}_4 \cdot 7\text{H}_2\text{O}$ ; analytical grade) and sodium hydroxide (NaOH;  
154 analytical grade) were used to synthesize Co-doped hausmannite. Potassium chloride  
155 (KCl; analytical grade) was used for PZC analysis. Di-sodium hydrogen arsenate  
156 ( $\text{Na}_2\text{HAsO}_4 \cdot 12\text{H}_2\text{O}$ ; analytical grade), sodium arsenite ( $\text{NaAsO}_2$ ; analytical grade) and  
157 sodium nitrate ( $\text{NaNO}_3$ ; analytical grade) were used to prepare the simulated  
158 wastewater. Potassium borohydride ( $\text{KBH}_4$ ; guaranteed reagent) and hydrochloric acid  
159 (HCl 32%; guaranteed reagent) were used for As(III) analysis. Potassium bromide (KBr;  
160 spectroscopically grade) was used for FTIR analysis. Deionized water (18 M $\Omega$  cm  
161 resistance) obtained from Aquapro Water Pro Ps was used to prepare stock solutions  
162 and wash the products for all experiments.

### 163 **1.2 Synthesis and characterization of Co-doped hausmannite**

164 Three Co-doped hausmannite samples with initial Co/Mn molar ratios of 0, 0.05  
165 and 0.10 (HM, CoH5 and CoH10) were prepared using the co-precipitation method  
166 (Giovannelli et al., 2012). The phase identification and determination of the basic  
167 physicochemical properties were described in detail in a previous study (Zhang et al.,  
168 2021).

169 The point of zero charge (PZC) of the as-prepared samples was determined with  
170 the salt addition method (Bhowmik et al., 2016). About 20 mL of 0.01 mol/L KCl  
171 solution was added to a series of 100 mL test tubes, and the solution pH values were

172 adjusted to 2.0–8.0, respectively, with 0.1 mol/L HCl or 0.1 mol/L NaOH solution, and  
173 recorded as the initial pH. Then, 0.0200 g of mineral was added to each tube, and the  
174 suspension was rotated thoroughly for 48 hr. At the end of reaction, the slurry was  
175 filtered and the pH of the filtrate was recorded as  $pH_f$ . The change of pH from  $pH_i$  to  
176  $pH_f$  ( $\Delta pH$ ) was plotted against  $pH_i$ ; the value of  $pH_i$  at which the  $\Delta pH$  was equal to zero  
177 represented the PZC of the tested solid.

### 178 **1.3 As(V) adsorption experiments**

179 Co-doped hausmannite samples (1 g) were suspended in 250 mL of 0.1 mol/L  
180  $NaNO_3$  solution for 24 hr to eliminate the effect of stirring and surface hydration, during  
181 which the pH was kept at  $4.5 \pm 0.05$ . About 10 mL of each mineral suspension was  
182 added to a 50 mL centrifuge tube, and then 0–3.2 mL of 10 mmol/L As(V) solution (pH  
183 4.5; containing 0.1 mol/L  $NaNO_3$  solution) was added, followed by the addition of 0.1  
184 mol/L  $NaNO_3$  solution to make a final reaction volume of 40 mL. These tubes were  
185 agitated mechanically in a shaker at  $25 \pm 2^\circ C$  for 24 hr. The ionic strength (0.01 mol/L,  
186 0.1 mol/L and 0.2 mol/L) and reaction pH (4.5, 5.5, 6.5 and 7.5) were measured. The  
187 mixture pH was adjusted to the required value by the addition of 0.1 mol/L  $HNO_3$  or  
188 NaOH solution during the reaction. At the end of the reaction, the suspensions were  
189 centrifuged, filtered, and the As(V) concentration in the filtrate was analyzed with the  
190 colorimetric method (Oscarson et al., 1980).

### 191 **1.4 As(III) oxidation experiments**

192 About 0.150 g of HM or CoH10 was added to 276 mL of 0.1 mol/L  $NaNO_3$   
193 solution at  $pH 4.50 \pm 0.05$  for aquotization for 24 hr. The As oxidation experiment was  
194 initiated by quick addition of 24 mL of 2.636 mmol/L  $NaAsO_2$  solution ( $pH = 4.50 \pm$   
195  $0.05$ ; with 0.1 mol/L  $NaNO_3$  solution) into the mineral suspension to make a final As  
196 concentration of 15.8 mg/L. The reaction was allowed to proceed at  $pH 4.50 \pm 0.05$  for  
197 24 hr. At certain time intervals, a 5 mL aliquot of mixture was taken and immediately  
198 filtered through a 0.22  $\mu m$  membrane. At the end of the reaction, the mixture was  
199 centrifuged. The As(III) and total As (As(T)) in the filtrate were measured by atomic  
200 fluorescence spectrometry (AFS) using 1.5% HCl -1.5%  $KBH_4$  and 5% HCl -2 %  $KBH_4$

201 as the carrying fluid. The concentration of As(V) in the solution was calculated by  
202 subtracting the As(III) concentration from As(T) in the solution. The concentrations of  
203 Mn(II) and Co(II) in the filtrate were determined by AAS.

204 The obtained solids at the end of reaction of As(III) oxidation and As(V)  
205 adsorption were washed thoroughly, and the wet pastes were covered with Kapton tape  
206 for XAFS analysis.

## 207 **1.5 X-ray absorption fine structure (XAFS) spectroscopy**

208 The XAFS data were collected on the 1W1B beamline at the Beijing Synchrotron  
209 Radiation Facility (BSRF) at room temperature (Yin et al., 2012). As K-edge XAFS  
210 data were collected in fluorescence mode over the energy range of 11635 to 12882 eV.  
211 Reduction and analysis of XAFS data were performed using Athena and Artemis from  
212 the Ifeffit software package (Ravel and Newville, 2006). As K-edge spectra were  
213 background-subtracted using the following parameters:  $E_0 = 11872$  eV,  $Rbkg = 1.0$  Å  
214 and  $k\text{-weight} = 2$ . Structural parameters (bond length ( $R$ ), coordination number ( $CN$ ),  
215 and Debye-Waller factor ( $\sigma^2$ )) for As were obtained by fitting the  $k^3$ -weighted EXAFS  
216 data to the standard EXAFS equation (Kelly et al., 2008). Phase and amplitude  
217 functions for single- and multi-scattering paths were calculated using Feff7.0 (Rehr et  
218 al., 1992). As K-edge EXAFS data were fitted in an R space of 1 to 4 Å over a k range  
219 of 3.4–12.4 Å<sup>-1</sup>, using several single scattering paths and one multiple scattering path  
220 calculated based on the structure of MnAsO<sub>4</sub> (ICSD 73489). An amplitude reduction  
221 factor ( $S_0^2$ ) of 0.978 for As was determined by fitting the As–O shell of Na<sub>3</sub>AsO<sub>4</sub> in an  
222 R range of 1–2 Å. In all fits, the number of independent variables was much smaller  
223 than that of independent data points allowed. During Fourier transformation and  
224 EXAFS data fitting, a Hanning window was used.

## 225 **2 Results**

### 226 **2.1 Basic physicochemical properties of Co-doped hausmannite**

227 The structure and basic physicochemical properties of the Co-doped hausmannite  
228 samples were described in detail in our previous paper (Zhang et al., 2021) and  
229 summarized in **Table 1**. With increasing doping amounts of Co, the Mn content

230 gradually decreased. The final Co/Mn molar ratios in these samples were 0.05 (CoH5)  
231 and 0.11 (CoH10). The Co-doped hausmannites consisted of cubic nanocrystals, and  
232 the TEM images showed that the average particle size was  $85 \pm 18$ ,  $131 \pm 27$  and  $103$   
233  $\pm 28$  nm for HM, CoH5 and CoH10, respectively (**Appendix A Fig. S1**). The increase  
234 in particle sizes of CoH5 and CoH10 resulted in slight decreases in specific surface area  
235 from  $12.4 \text{ m}^2/\text{g}$  to  $11.7\text{--}11.8 \text{ m}^2/\text{g}$ . The PZC of HM was  $7.04 \pm 0.03$  (**Appendix A Fig.**  
236 **S2**), and Co doping resulted in a slight decrease in PZC, consistent with reports that the  
237 PZC of Co compounds, including CoOOH and Co<sub>2</sub>O<sub>3</sub>, is 6.9 and 6.2, respectively  
238 (Kosmulski, 2009).

## 239 **2.2 As(V) adsorption at the mineral-water interface**

240 The effects of ionic strength and pH on the As(V) adsorption by the Co-doped  
241 hausmannite samples were systematically analyzed (**Fig. 1a**). With increasing NaNO<sub>3</sub>  
242 concentration from 0.01 mol/L to 0.2 mol/L, the As(V) adsorption density on HM  
243 remained almost constant at a given pH. By contrast, at a given ionic strength, pH  
244 greatly affected As(V) adsorption; as pH increased from 4.5 to 7.5, the As(V)  
245 adsorption density decreased from 5.29–5.61 mg/g to 0.13–0.19 mg/g (**Fig. 1a**). Similar  
246 results have been reported for As(V) and Cr(VI) adsorption on hausmannite at pH 2–8  
247 (Barreto et al., 2020; Cantu et al., 2014; Garcia et al., 2014). This strong pH dependency  
248 of As(V) adsorption can be mainly ascribed to the reduced competition between As(V)  
249 and OH<sup>-</sup> for surface sites at lower pH. According to the dissociation constants of  
250 H<sub>3</sub>AsO<sub>4</sub> ( $pK_1 = 2.26$ ,  $pK_2 = 6.76$  and  $pK_3 = 11.29$ ) (Lide and Haynes, 2010), As(V)  
251 mainly exists as anionic As species of H<sub>2</sub>AsO<sub>4</sub><sup>-</sup> and HAsO<sub>4</sub><sup>2-</sup> in the tested pH range.

252 Adsorption isotherm experiments were conducted with initial As(V)  
253 concentrations of 0–60 mg/L (**Fig. 1b**). With increasing As(V) concentration, the As(V)  
254 adsorption first showed a sharp increase, and then leveled off at high  
255 As(V) concentrations. Co-doped hausmannite samples showed similar As(V)  
256 adsorption behaviors as HM; however, the As(V) removal by Co-doped samples from  
257 the solution gradually decreased with increasing Co doping level. Analyses of the  
258 isotherm adsorption data with the Langmuir and Freundlich adsorption models (**Fig. 1b**

259 **and Appendix A Table S1)** revealed that the Freundlich model significantly better fit  
260 the data than did the Langmuir model, suggesting that the active sites on the Co-doped  
261 samples are energetically heterogeneous. The  $k$  values obtained from the Freundlich  
262 model fitting indicated that the adsorption capacity of CoH10 for As(V) was about 36%  
263 lower than that of HM. This decrease in adsorption capacity may be ascribed to the  
264 decrease in PZC of Co-doped hausmannite, indicating that the decrease in positive  
265 charge is unfavorable for As(V) adsorption.

### 266 **2.3 As(III) oxidation at the mineral-water interface**

267 In the pH range of most natural waters, soils and sediments, As(III) usually exists  
268 as neutral  $\text{H}_3\text{AsO}_3$  molecules, while As(V) usually exists in the forms of  $\text{H}_2\text{AsO}_3^-$  and  
269  $\text{HAsO}_3^{2-}$  anions, which can be readily adsorbed onto the mineral surfaces. Therefore,  
270 As(III) has higher mobility and ecological toxicity than As(V). We, therefore,  
271 investigated the effect of Co doping on the interaction between hausmannite and As(III).  
272 The As oxidation experiments were conducted by the reaction of the solutions  
273 containing As(III) (15.8 mg/L) and HM (0.5 g/L) in air atmosphere at 25°C and pH 4.5.  
274 The control experiment was also conducted under the same conditions, but under  $\text{N}_2$ ,  
275 to investigate the effect of  $\text{O}_2$  on the oxidation of As(III) to As(V) (**Appendix A Fig.**  
276 **S3**). In both atmospheres, the As(V) concentrations in the solutions were almost the  
277 same, indicating that  $\text{O}_2$  in air has a negligible effect on As(III) oxidation by  
278 hausmannite.

279 **Figures 2a, b** present the plots of concentrations of various As species in the  
280 reaction systems with time. The amount of As(V) in the solution gradually increased,  
281 confirming the oxidation of As(III) by Mn(III) (Song et al., 2020; Song et al., 2021).  
282 Concurrently, As(III) in the solution was quickly depleted, which could be attributed to  
283 the oxidation of As(III) to As(V) and the adsorption of As(V) onto the mineral surface.  
284 The adsorption of both As(III) and As(V), generated by oxidation, contributed to the  
285 decrease in total As in the solution. For all the reactions, the concentrations of the As  
286 species approached equilibrium after 2 hr, which may be ascribed to the effect of surface  
287 passivation. Hausmannite has a high PZC, and thus its surface is positively charged at

288 pH 4.5 and can adsorb large amounts of As species, which eventually leads to the  
289 blocking of the active sites. At equilibrium, As adsorption and fixation on the mineral  
290 surface were the dominant process, and the As in the solution was mostly As(V). At the  
291 end of the reaction, the amount of As adsorbed and fixed on the mineral surface was  
292  $13.24 \pm 0.66$  mg/L for HM and  $12.16 \pm 0.70$  mg/L for CoH10. The total concentration  
293 of As(V) in the solution and adsorbed/fixed on the mineral surface was almost the same  
294 for HM ( $15.58 \pm 0.71$  mg/L) and CoH10 ( $15.43 \pm 0.75$  mg/L), which accounted for  $99$   
295  $\pm 4\%$  and  $98 \pm 5\%$  of the initial amount of added As(III), respectively. The oxidation  
296 capacities of HM and CoH10 for As(III) were  $416 \pm 19$  mmol/kg and  $412 \pm 20$  mmol/kg,  
297 respectively.

298 The As(III) oxidation rate was quantified by fitting the reaction data over 0–0.5 hr  
299 using a pseudo-first order kinetic model (**Fig. 2c**). The As(III) oxidation rate constants  
300 for HM and CoH10 were  $0.0504 \pm 0.0011$  min<sup>-1</sup> and  $0.0219 \pm 0.0012$  min<sup>-1</sup>, respectively.  
301 The differences in oxidation rate between the samples may be ascribed to several  
302 reasons. Firstly, TEM analysis showed that CoH10 had a larger particle size and  
303 therefore a lower active site density than HM (Zhang et al., 2009). Another possible  
304 reason is that the crystal field stabilization energy (CFSE) of low-spin Co(III) ion (534.2  
305 kJ/mol) is higher than that of Mn(III) (150.8 kJ/mol), and thus the Co(III)-O bond has  
306 higher binding energy than the Mn(III)/Mn(II)-O bond, resulting in greater activation  
307 energy at these Co(III) sites, and correspondingly a slower reaction rate (Yin et al.,  
308 2011).

309 During the As(III) oxidation by these Co-doped samples under the experimental  
310 conditions, large amounts of Mn(II) and Co(II) were released. In the CoH10 mineral  
311 suspension obtained by the addition of 0.1 M NaNO<sub>3</sub> solution to reach a final solid-to-  
312 liquid ratio of 0.5 g/L and equilibrated at pH 4.5 for 24 hr, the concentrations of Mn(II)  
313 and Co(II) were  $148 \pm 0.1$  mg/L and  $19 \pm 0.03$  mg/L, respectively. After the addition  
314 of As(III), the release of Mn(II) and Co(II) was only slightly increased. The highest  
315 Mn(II) and Co(II) concentration was measured as  $\sim 160$  mg/L and  $\sim 21$  mg/L,  
316 respectively (**Fig. 2d**).

## 317 **2.4 Mechanism for the binding of As on mineral surface**

### 318 **2.4.1 FTIR analysis of HM before and after As(III) oxidation**

319 In order to determine the mechanism for the binding of As on the hausmannite  
320 surface, FTIR analysis was conducted on a typical sample after reaction with As(III)  
321 (HM\_0.8As(III)) (**Fig. 3**). Compared with the spectrum of pristine HM, the spectrum  
322 of HM\_0.8 As(III) clearly showed an additional peak at  $750\text{ cm}^{-1}$ . This peak matched  
323 that reported for an in-situ ATR-FTIR analysis of As(III) reaction with hausmannite  
324 (Song et al., 2020; Song et al., 2021), which corresponds to the vibration of As(V)-O-  
325 Mn(III), indicating the formation of As(V) bidentate binuclear surface complexes on  
326 the mineral surface.

### 327 **2.4.2 Arsenic K-edge XAFS analysis**

328 The As K-edge XAFS spectra of HM and CoH10 after As(V) adsorption and  
329 As(III) oxidation were analyzed to investigate the surface As valence and local bonding  
330 structure on the mineral surface. A comparison of the As K-edge XANES spectra of the  
331 samples with those of As(III) and As(V) standards ( $\text{As}_2\text{O}_3$  and  $\text{Na}_3\text{AsO}_4$ ) demonstrated  
332 that only As(V) was bound to HM and CoH10 surfaces during As(V) adsorption and  
333 As(III) oxidation experiments (**Fig. 4**). This result is consistent with the XANES,  
334 Raman and infrared analyses of hausmannite after As(III) oxidation in previous studies,  
335 which demonstrated that As was adsorbed in the form of As(V) (Silva et al., 2013; Silva  
336 et al., 2012).

337 The EXAFS spectra for all of the As-loaded hausmannite samples showed similar  
338 oscillations, indicating that they had similar local atomic structures. However, these  
339 spectra were different from those of  $\text{Na}_3\text{AsO}_4$  (**Fig. 5A**), which was especially obvious  
340 in the corresponding FTs (**Fig. 5B**). Each of the FTs showed a major peak at  $R+\Delta R \sim$   
341  $1.3\text{ \AA}$ , which can be assigned to the As-O shell in the  $[\text{AsO}_4]$  unit. Additionally, there  
342 was a peak at  $R+\Delta R \sim 2.9\text{ \AA}$  in As-loaded hausmannite, but this peak was absent in the  
343 spectrum of  $\text{Na}_3\text{AsO}_4$ , suggesting that As forms inner-sphere complexes on the mineral  
344 surface.

345 Fittings of the As K-edge EXAFS spectra for the hausmannite samples yielded As-

346 O distances ranging from 1.68–1.72 Å (**Fig. 5** and **Table 2**). These distances are  
347 identical to the previously reported As(V)-O distances for As(V) associated with Mn-  
348 oxides and Fe-oxides (Foster et al., 2003; Lafferty et al., 2010; Manning et al., 2002;  
349 Zhang et al., 2014), but shorter than the As(III)-O distance (1.75–1.77 Å) for NaAsO<sub>2</sub>  
350 or As(III) adsorbed on FeOOH (Zhang et al., 2014). This is consistent with the XANES  
351 results showing that As was adsorbed on the mineral surface in the form of As(V). Only  
352 a single As-Mn distance of 3.25–3.30 Å is needed to fit the  $R+\Delta R \sim 2.9$  Å peak.

353 In a previous study of As(V) adsorption on the birnessite surface, bidentate-  
354 mononuclear (BM,  $R \sim 2.7$  Å), bidentate-binuclear (BB,  $R \sim 3.1$ – $3.2$  Å) and  
355 monodentate-mononuclear (MM,  $R \sim 3.4$ – $3.5$  Å) complexes were identified (Lafferty et  
356 al., 2010). However, the analysis of BM complexes revealed that As-O multiple  
357 scattering may also contribute to the  $R \sim 2.7$  Å peak (Sherman and Randall, 2003). In  
358 the present study, an As-O multiple scattering path was added for the fitting and no BM  
359 complex was found, which is consistent with a previous finding about the binding  
360 mechanism of As on birnessite in the presence of Fe(II) (Wu et al., 2018). During the  
361 As(III) oxidation by birnessite in a stirred-flow system, the Mn(III) content gradually  
362 increased. The binding of As(V) to Mn(III) sites probably contributed to the observed  
363 increase in BB As-Mn distance from 3.12–3.13 Å to 3.19–3.23 Å, and the decrease in  
364 MM As-Mn distance from 3.42–3.47 Å to 3.34 Å (Lafferty et al., 2010). The As(V)  
365 retained on the Ni-doped hausmannite surface during As(V) adsorption and As(III)  
366 oxidation resulted in an As-Mn distance of 3.28–3.35 Å, as determined by EXAFS  
367 fitting, which could be assigned to the formation of BB complex on Mn(III) sites (Song  
368 et al., 2020). A quantum chemical study of As(V) adsorption on Mn(III) sites in Mn  
369 oxides also indicated an As-Mn distance of 3.29–3.47 Å for BB configuration (Zhu et  
370 al., 2009). Hence, the observed As-Mn distance on Co-doped hausmannite surface  
371 could be reasonably assigned to the formation of BB complexes.

## 372 **3 Discussion**

### 373 **3.1 As(V) adsorption mechanism**

374 Among various Mn oxides, hausmannite has a relatively high adsorption capacity

375 for certain anions (Li and Jaisi, 2015). Our experiments of As(V) adsorption onto Co-  
376 doped hausmannite demonstrated that pH has a great impact on As(V) adsorption, but  
377 ionic strength has almost no effect at pH ranging from 4.5 to 7.5 (**Fig. 1a**). However,  
378 other studies suggested that the binding of As(V) onto hausmannite at pH 3 is  
379 suppressed by the presence of  $\text{NO}_3^-$  at concentrations  $> 3$  ppm (Garcia et al., 2014),  
380 possibly because a lower pH such as pH 3 can enhance the dissolution of the mineral  
381 compared with a high pH (Luo et al., 2018).

382 For As(V)-adsorbed hausmannite, no As(III) was detected on the mineral surface  
383 by As K-edge XANES analysis, suggesting that no As(V) reduction occurred during  
384 adsorption under the experimental conditions in this study, which is the same as  
385 observed for As(V) adsorption on Ni-doped hausmannite (Song et al., 2020). However,  
386 in a previous study, Cr K-edge XANES analysis of Cr(VI) adsorbed on hausmannite at  
387 pH 2, 4 and 6 for 1 hr demonstrated that Cr(VI) was reduced to Cr(III), owing to the  
388 electron transfer from Mn(II) to Cr(VI) (Hernandez, 2010). This difference between  
389 As(V) and Cr(VI) adsorption behaviors on hausmannite may be attributed to the lower  
390 standard reduction potential of  $\text{H}_3\text{AsO}_4/\text{HAsO}_2$  ( $E^0 = 0.56$  V) relative to that of  $\text{HCrO}_4^-$   
391  $/\text{Cr(III)}$  ( $E^0 = 1.35$  V) (Lide and Haynes, 2010). Additionally, the reduction of Cr(VI)  
392 on the mineral surface may also be related to the interaction with the X-ray beam  
393 irradiation during the analysis, as in the reduction of Np(V) by the X-ray beam during  
394 XAFS analysis of Np(V) adsorption on hausmannite (Wilk et al., 2005).

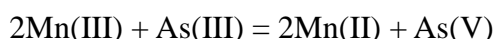
395 Furthermore, the As K-edge EXAFS analysis demonstrated an As-Mn distance of  
396 3.25–3.26 Å for As(V) adsorbed on the Co-doped hausmannite surface, which  
397 corresponds to the BB inner sphere complex. Raman and IR analysis of As(V)-loaded  
398 hausmannite showed that the anions were adsorbed as both monodentate- and bidentate-  
399 mononuclear complexes at pH 5 (Silva et al., 2013). Recently, an ATR-FTIR study of  
400 As(V) adsorption onto hausmannite demonstrated that low pH and high As(V) surface  
401 loading are favorable for the formation of outer-sphere or hydrogen-bonded surface  
402 complexes and inner-sphere monodentate species on mineral surfaces, while high pH  
403 and low surface loading are conducive to the formation of bidentate complexes (Barreto

404 et al., 2020). Another ATR-FTIR study suggested that many types of complexes, such  
405 as bidentate, monodentate, binuclear, and mononuclear moieties as well as their  
406 protonated forms, are all possibly formed on the mineral surface (Song et al., 2020).  
407 However, this is different from the EXAFS results, which indicated that the As(V)  
408 adsorbed on the mineral surface forms BB complexes (Song et al., 2020). Our EXAFS  
409 results confirm the formation of BB complexes. The inconsistency in the results of  
410 EXAFS and ATR-FTIR can be mainly ascribed to the fact that EXAFS detects the  
411 average overall information but in-situ ATR-FTIR acquires information from the  
412 surface and is more sensitive to the effects of protonation. Thus, the combination of  
413 EXAFS and in-situ ATR-FTIR is needed in future studies of interface reactions.

### 414 **3.2 As(III) oxidation mechanism**

415 Our results showed that Co-doped hausmannite has high oxidation capacity for  
416 As(III), and a large part of the generated As(V) is adsorbed on the mineral surface.  
417 Furthermore, the solution pH increased during the reaction. For example, the final pH  
418 in the CoH10 system increased to ~5.2, indicating the consumption of H<sup>+</sup> during the  
419 reaction (Feng et al., 2006; Silva et al., 2012).

420 In hausmannite, structural Mn(III) is responsible for As(III) oxidation according  
421 to the following equation:



422 According to the equation, 2 mol of Mn(II) will be released into the solution when  
423 1 mol of As(III) is oxidized. In previous studies, for the As(III) oxidation by  
424 hausmannite doped with 0, 1 wt.% and 2.8 wt.% Co, the Mn(II): As(V) ratios were  
425 determined to be 1.5:1, 1.7:1 and 2.0:1, respectively, which are also consistent with the  
426 results obtained for Ni-doped hausmannite (Song et al., 2020; Song et al., 2021). In the  
427 present study, before the addition of As(III), the mineral was partially dissolved,  
428 resulting in the release of 45% of the total Mn and ~57% of the total Co in CoH10  
429 during equilibration at pH 4.5 for 24 hr. During As(III) oxidation, additional ~12 mg/L  
430 of Mn(II) and ~2 mg/L of Co(II) were released. The molar ratio of Mn(II) in the solution  
431 to total As(V) produced (including both As(V) in the solution and that adsorbed/fixe

432 on mineral surface) was estimated to be 1:1. The low Mn(II) concentration in the  
433 solution might be due to the re-adsorption on the As(V)-loaded mineral surface. In a  
434 previous study, less than 25% of total As was adsorbed on mineral surface (Song et al.,  
435 2020), while in the present study,  $77 \pm 4\%$  of total As was adsorbed and fixed on the  
436 mineral surface in the form of As(V) (**Fig. 2**). At pH 4.5, As(V) exists predominantly  
437 in the form of  $\text{H}_2\text{AsO}_4^-$  (Lide and Haynes, 2010). The retention of a large amount of  
438 anions on the mineral surface would neutralize the positive charge and make the zeta  
439 potential ( $\zeta$ ) more negative, which is more favorable for the re-adsorption of Mn(II) and  
440 Co(II).

441 Our As K-edge XAFS analysis of the As-loaded samples after As(III) oxidation  
442 showed that As was adsorbed on the mineral surface as As(V) by forming the BB  
443 complexes with the nearest As-Mn distance of 3.28–3.30 Å, which is consistent with  
444 previous studies (Song et al., 2020). These As species were relatively stable on the  
445 mineral surface, and the amount of As adsorbed and fixed on the mineral surface was  
446 almost constant after reaching reaction equilibrium (**Fig. 2**). All these results suggest  
447 that hausmannite may greatly affect the geochemical behaviors of As(III), by oxidation  
448 of As(III) to As(V), and by adsorption of As(V) on the mineral surface.

449 In fact, hausmannite nanomaterials have been used to remediate As(III)-polluted  
450 soils and sediments. For example, hausmannite was added to two paddy soils to enhance  
451 arsenite oxidation, leading to a decrease in As concentration in rice grains and straw  
452 (Xu et al., 2017). In natural environments, Mn oxides may contain significant amounts  
453 of metal impurities. The present study revealed that although incorporation of Co into  
454 hausmannite decreased the initial As(III) oxidation rate, the overall oxidation capacities  
455 of the various doped samples were similar. Therefore, natural hausmannite may also be  
456 highly oxidizing towards low valence redox-sensitive trace elements. However, it is  
457 necessary to continue to study reactions of hausmannite with these elements in the  
458 presence of coexisting ions, organic molecules and humic substances.

#### 459 **4 Conclusions**

460 After Co doping, hausmannite showed a decrease in PZC and high reactivity for

461 As(III) oxidation and As(V) adsorption. Ionic strength had no effect on the adsorption  
462 of As(V) onto the mineral surface, while an increase in the reaction pH from 4.5 to 7.5  
463 gradually decreased the adsorption capacity. The As(V) adsorption capacity gradually  
464 decreased with increasing Co doping level. Co-doped hausmannite has high oxidation  
465 activities for As(III), and most of the generated As(V) is adsorbed on the mineral  
466 surface. Although Co doping decreased the initial oxidation rate, the overall oxidation  
467 capacity of the Co-doped hausmannite was comparable to that of pristine hausmannite.  
468 The As species in hausmannite after both As(V) adsorption and As(III) oxidation  
469 probably form bidentate binuclear complexes with the nearest As-Mn distance of 3.25–  
470 3.30 Å. These results suggest that natural hausmannite may play an important role in  
471 mediating the geochemical cycling of As in surficial environments.

472

### 473 **Acknowledgments**

474 The authors gratefully thank the Key science and technology projects of Inner Mongolia  
475 autonomous region (2019ZD001), the National Natural Science Foundations of China  
476 (Nos.42077015, 41771267 and 41877030), the National Key Research and  
477 Development Program of China (No. 2016YFD0800403), and the Fundamental  
478 Research Funds for the Central Universities (Grant 103-510320036) for the financial  
479 support.

480

### 481 **Appendix A. Supplementary data**

482 Supplementary data associated with this article can be found in the online version at  
483 xxxxxx.

484

### 485 **References**

- 486 Antao, S.M., Cruickshank, L.A., Hazrah, K.S., 2019. Structural trends and solid-  
487 solutions based on the crystal chemistry of two hausmannite (Mn<sub>3</sub>O<sub>4</sub>) samples  
488 from the Kalahari Manganese Field. *Minerals* 9:343.
- 489 Baron, V., Gutzmer, J., Rundlof, H., Tellgren, R., 1998. The influence of iron

490 substitution on the magnetic properties of hausmannite,  $\text{Mn}^{2+}(\text{Fe,Mn})_2(\text{Fe}^{3+})\text{O}_4$ .  
491 Am. Mineral. 83:786-793.

492 Barreto, M.S.C., Elzinga, E.J., Alleoni, L.R.F., 2020. Hausmannite as potential As(V)  
493 filter. Macroscopic and spectroscopic study of As(V) adsorption and desorption  
494 by citric acid. Environ. Pollut. 262:114196.

495 Bhowmik, K.L., Debnath, A., Nath, R.K., Das, S., Chattopadhyay, K. K., Saha, B., 2016.  
496 Synthesis and characterization of mixed phase manganese ferrite and hausmannite  
497 magnetic nanoparticle as potential adsorbent for methyl orange from aqueous  
498 media: Artificial neural network modeling. J. Mol. Liq. 219:1010-1022.

499 Bordeneuve, H., Tenailleau, C., Guillemet-Fritsch, S., Smith, R., Suard, E., Rousset, A.,  
500 2010. Structural variations and cation distributions in  $\text{Mn}_{3-x}\text{Co}_x\text{O}_4$  ( $0 \leq x \leq 3$ )  
501 dense ceramics using neutron diffraction data. Solid State Sci. 12:379-386.

502 Cantu, Y., Remes, A., Reyna, A., Martinez, D., Villarreal, J., Ramos, H., et al., 2014.  
503 Thermodynamics, kinetics, and activation energy studies of the sorption of  
504 chromium(III) and chromium(VI) to a  $\text{Mn}_3\text{O}_4$  nanomaterial. Chem. Eng. J.  
505 254:374-383.

506 Choong, T.S.Y., Chuah, T.G., Robiah, Y., Koay, F.L.G., Azni, I., 2007. Arsenic toxicity,  
507 health hazards and removal techniques from water: an overview. Desalination  
508 217:139-166.

509 Dong, R., Ye, Q., Kuang, L., Lu, X., Zhang, Y., Zhang, X., et al., 2013. Enhanced  
510 supercapacitor performance of  $\text{Mn}_3\text{O}_4$  nanocrystals by doping transition-metal  
511 ions. ACS Appl. Mater. Inter. 5:9508-9516.

512 Feng, X., Zu, Y., Tan, W., Liu, F., 2006. Arsenite oxidation by three types of manganese  
513 oxides. J. Environ. Sci. 18:292-298.

514 Foster, A.L., Brown, G.E., Parks, G.A., 2003. X-ray absorption fine structure study of  
515 As(V) and Se(IV) sorption complexes on hydrous Mn oxides. Geochim.  
516 Cosmochim. Acta 67:1937-1953.

517 Garcia, S., Sardar, S., Maldonado, S., Garcia, V., Tamez, C., Parsons, J.G., 2014. Study  
518 of As(III) and As(V) oxoanion adsorption onto single and mixed ferrite and

519 hausmannite nanomaterials. *Microchem. J.* 117:52-60.

520 Giovannelli, F., Autret-Lambert, C., Mathieu, C., Chartier, T., Delorme, F., Seron, A.,  
521 2012. Synthesis of manganese spinel nanoparticles at room temperature by  
522 coprecipitation. *J. Solid State Chem.* 192:109-112.

523 Habuda-Stanic, M., Nujic, M., 2015. Arsenic removal by nanoparticles: a review.  
524 *Environ. Sci. Pollut. Res. Int.* 22:8094-8123.

525 Hernandez, J., 2010. Chromium(III/VI) binding to magnetite, hausmannite, and  
526 jacobsite nanomaterials. PhD thesis. The University of Texas at El Paso.  
527 AAI1479558.

528 Jha, A., Thapa, R., Chattopadhyay, K.K., 2012. Structural transformation from  $Mn_3O_4$   
529 nanorods to nanoparticles and band gap tuning via Zn doping. *Mater. Res. Bull.*  
530 47:813-819.

531 Kelly, S.D., Hesterberg, D., Ravel, B., 2008. Analysis of soils and minerals using X-  
532 ray absorption spectroscopy, in: Ulrey A L, Drees R L (Eds.), *Methods of Soil*  
533 *Analysis, Part 5-Mineralogical Methods.* Soil Science Society of America,  
534 Wisconsin, pp. 387-463.

535 Kosmulski, M., 2009. pH-dependent surface charging and points of zero charge. IV.  
536 Update and new approach. *J. Colloid Interf. Sci.* 337:439-448.

537 Lafferty, B.J., Ginder-Vogel, M., Zhu, M., Livi, K.J.T., Sparks, D.L., 2010. Arsenite  
538 oxidation by a poorly crystalline manganese-oxide. 2. Results from X-ray  
539 absorption spectroscopy and X-ray diffraction. *Environ. Sci. Technol.* 44:8467-  
540 8472.

541 Li, H., Jaisi, D.P., 2015. An isotope labeling technique to investigate atom exchange  
542 during phosphate sorption and desorption. *Soil Sci. Soc. Am. J.* 79:1340-1351.

543 Lide, D.R., Haynes, W. M., 2010. *CRC Handbook of Chemistry and Physics*, (90th ed.).  
544 CRC Press: Florida.

545 Luo, Y., Tan, W., Suib, S.L., Qiu, G., Liu, F., 2018. Dissolution and phase  
546 transformation processes of hausmannite in acidic aqueous systems under anoxic  
547 conditions. *Chem. Geol.* 487:54-62.

548 Manning, B.A., Fendorf, S.E., Bostick, B., Suarez, D.L., 2002. Arsenic(III) oxidation  
549 and Arsenic(V) adsorption reactions on synthetic birnessite. *Environ. Sci. Technol.*  
550 36:976-981.

551 Oscarson, D.W., Huang, P.M., Liaw, W.K., 1980. The oxidation of arsenite by aquatic  
552 sediments. *J. Environ. Qual.* 9:4:700-703.

553 Parsons, J.G., Lopez, M.L., Peralta-Videa, J.R., Gardea-Torresdey, J.L., 2009.  
554 Determination of arsenic(III) and arsenic(V) binding to microwave assisted  
555 hydrothermal synthetically prepared Fe<sub>3</sub>O<sub>4</sub>, Mn<sub>3</sub>O<sub>4</sub>, and MnFe<sub>2</sub>O<sub>4</sub> nanoadsorbents.  
556 *Microchem. J.* 91:100-106.

557 Peña, J., Duckworth, O.W., Bargar, J.R., Sposito, G., 2007. Dissolution of hausmannite  
558 (Mn<sub>3</sub>O<sub>4</sub>) in the presence of the trihydroxamate siderophore desferrioxamine B.  
559 *Geochim. Cosmochim. Acta* 71:5661-5671.

560 Ravel, B., Newville, M., 2006. ATHENA and ARTEMIS: Interactive graphical data  
561 analysis using IFEFFIT. *Phys. Scr.* 115, 1007-1010.

562 Rehr, J.J., Albers, R.C., Zabinsky, S.I., 1992. High-order multiple-scattering  
563 calculations of X-ray-absorption fine structure. *Phys. Rev. Lett.* 69:3397-3400.

564 Şahin, B., Aydin, R., Cetin, H., 2020. Tuning the morphological, structural, optical and  
565 dielectric properties of hausmannite (Mn<sub>3</sub>O<sub>4</sub>) films by doping heavy metal lead.  
566 *Superlattice. Microst.* 143:106546.

567 Shaughnessy, D.A., Nitsche, H., Booth, C.H., Shuh, D.K., Waychunas, G.A., Wilson,  
568 R.E., et al., 2003. Molecular interfacial reactions between Pu(VI) and manganese  
569 oxide minerals manganite and hausmannite. *Environ. Sci. Technol.* 37:3367-3374.

570 Sherman, D.M., Randall, S.R., 2003. Surface complexation of arsenic(V) to iron(III)  
571 (hydr)oxides: structural mechanism from ab initio molecular geometries and  
572 EXAFS spectroscopy. *Geochim. Cosmochim. Acta* 67:4223-4230.

573 Silva, G.C., Almeida, F.S., Dantas, M.S., Ferreira, A.M., Ciminelli, V.S., 2013. Raman  
574 and IR spectroscopic investigation of As adsorbed on Mn<sub>3</sub>O<sub>4</sub> magnetic composites.  
575 *Spectrochim Acta A* 100:161-165.

576 Silva, G.C., Almeida, F.S., Ferreira, A.M., Ciminelli, V.S.T., 2012. Preparation and

577 application of a magnetic composite ( $Mn_3O_4/Fe_3O_4$ ) for removal of As(III) from  
578 aqueous solutions. *Mat. Res.* 15:403-408.

579 Song, B., Cerkez, E.B., Elzinga, E.J., Kim, B., 2020. Effects of Ni incorporation on the  
580 reactivity and stability of hausmannite ( $Mn_3O_4$ ): Environmental implications for  
581 Mn, Ni, and As solubility and cycling. *Chem. Geol.* 558:119862.

582 Song, B., Cerkez, E.B., Elzinga, E.J., Kim, B., 2021. Effects of structural cobalt on the  
583 stability and reactivity of hausmannite and manganite: Cobalt coordination  
584 chemistry and arsenite oxidation. *Chem. Geol.*:120453.

585 Weaver, R.M., Hochella, M.F., 2003. The reactivity of seven Mn-oxides with  $Cr^{3+}_{aq}$ : A  
586 comparative analysis of a complex, environmentally important redox reaction. *Am.*  
587 *Mineral.* 88:2016-2027.

588 Wilk, P.A., Shaughnessy, D.A., Wilson, R.E., Nitsche, H., 2005. Interfacial interactions  
589 between Np(V) and manganese oxide minerals manganite and hausmannite.  
590 *Environ. Sci. Technol.* 39:2608-2615.

591 Wu, Y., Kukkadapu, R.K., Livi, K.J.T., Xu, W.Q., Li, W., Sparks, D.L., 2018. Iron and  
592 arsenic speciation during As(III) oxidation by manganese oxides in the presence  
593 of Fe(II): Molecular-level characterization using XAFS, Mossbauer, and TEM  
594 Analysis. *Acs Earth Space Chem.* 2:256-268.

595 Xu, X., Chen, C., Wang, P., Kretzschmar, R., Zhao, F.J., 2017. Control of arsenic  
596 mobilization in paddy soils by manganese and iron oxides. *Environ. Pollut.*  
597 231:37-47.

598 Yin, H., Feng, X.H., Qiu, G.H., Tan, W.F., Liu, F., 2011. Characterization of Co-doped  
599 birnessites and application for removal of lead and arsenite. *J. Hazard. Mater.*  
600 188:341-349.

601 Yin, H., Sun, J., Yan, X., Yang, X., Feng, X., Tan, W., et al., 2020. Effects of Co(II) ion  
602 exchange, Ni(II)- and V(V)-doping on the transformation behaviors of Cr(III) on  
603 hexagonal turbostratic birnessite-water interfaces. *Environ. Pollut.* 256:113462.

604 Yin, H., Tan, W.F., Zheng, L.R., Cui, H.J., Qiu, G.H., Liu, F., et al., 2012.  
605 Characterization of Ni-rich hexagonal birnessite and its geochemical effects on

606 aqueous  $Pb^{2+}/Zn^{2+}$  and As(III). *Geochim. Cosmochim. Acta* 93:47-62.  
607 Zhang, G., Liu, F., Liu, H., Qu, J., Liu, R., 2014. Respective role of Fe and Mn oxide  
608 contents for arsenic sorption in iron and manganese binary oxide: An X-ray  
609 absorption spectroscopy investigation. *Environ. Sci. Technol.* 48:10316-10322.  
610 Zhang, H.Z., Chen, B., Banfield, J.F., 2009. The size dependence of the surface free  
611 energy of titania nanocrystals. *Phys. Chem. Chem. Phys.* 11:2553-2558.  
612 Zhang, S., Li, H., Wu, Z., Post, J.E., Lanson, B., Elzinga, E.J., et al., 2021. Effects of  
613 Co doping on the structure and physicochemical properties of hausmannite  
614 ( $Mn_3O_4$ ) and its transformation during aging. *Chem. Geol.* 582:120448.  
615 Zhu, M., Paul, K.W., Kubicki, J.D., Sparks, D.L., 2009. Quantum chemical study of  
616 Arsenic(III, V) adsorption on Mn-oxides: Implications for Arsenic(III) oxidation.  
617 *Environ. Sci. Technol.* 43:6655-6661.

618

619

620

621

622

623

624

625

626

627

628

629

630

631

632

633

634

635

636

637

638

639

640 **List of tables**641 **Table 1** Chemical composition, specific surface area (SSA) and point of zero charge

642 (PZC) of Co-doped hausmannite samples.

Sample	Element content (wt%)		Co/Mn at. %	SSA (m <sup>2</sup> /g)	PZC
	Mn	Co			
HM	70.92(1)	0	0	12.4 ± 0.1	7.04(3)
CoH5	69.63(32)	3.52(5)	5	11.7 ± 0.2	6.92(1)
CoH10	65.93(116)	6.70(11)	11	11.8 ± 0.1	6.86(4)

643

644 **Table 2.** Structural parameters obtained from the fitting of As K-edge EXAFS for

645 typical samples after As(V) adsorption and As(III) oxidation.

Sample	shell	CN	R (Å)	$\sigma^2$	$\Delta E$ (eV)	R factor
HM_0.05As(V)	As-O	4.9(6)	1.695(7)	0.0025(9)	8.3(20)	0.0282
	As-Mn	0.7(9)	3.295(26)	0.0016(67)		
HM_0.4As(V)	As-O	4.9(6)	1.686(7)	0.0031(9)	6.0(22)	0.0272
	As-Mn	0.5(11)	3.263(47)	0.0040(122)		
CoH10_0.05As(V)	As-O	4.8(7)	1.688	0.0029	6.4(23)	0.0359
	As-Mn	0.9(4)	3.251(26)	0.0023(17)		
CoH10_0.4As(V)	As-O	4.1(7)	1.682	0.0014	4.9(29)	0.0459
	As-Mn	0.5	3.263(39)	0.0012(104)		
HM_0.8As(III)	As-O	3.9(5)	1.716(7)	0.0020(9)	13.4(20)	0.0388
	As-Mn	0.6(4)	3.277(39)	0.0006(19)		
CoH10_0.8As(III)	As-O	4.6(6)	1.697	0.0027	10.0(23)	0.0401

646

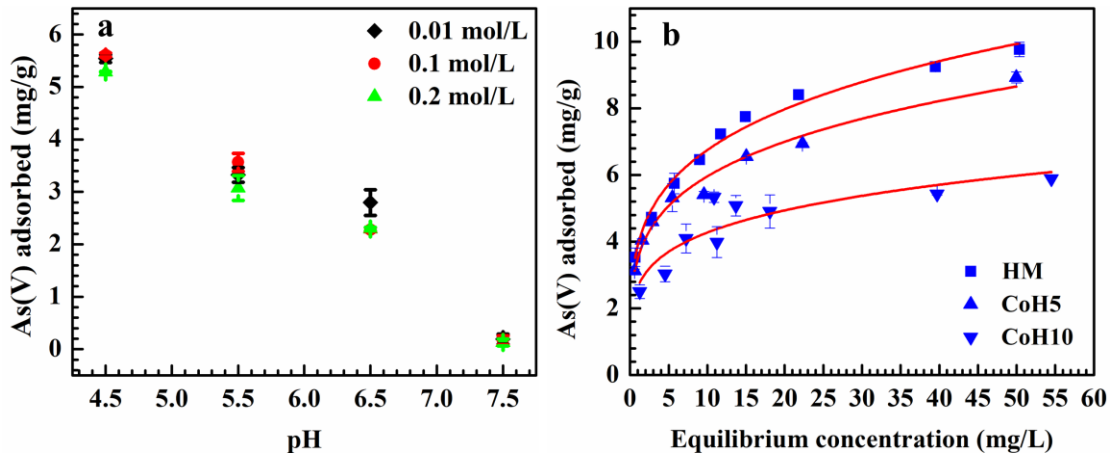
647

648

649

650

## 651 List of figures



652

653 **Fig. 1** (a) Effects of pH and ionic strength on As(V) adsorption on HM with an initial

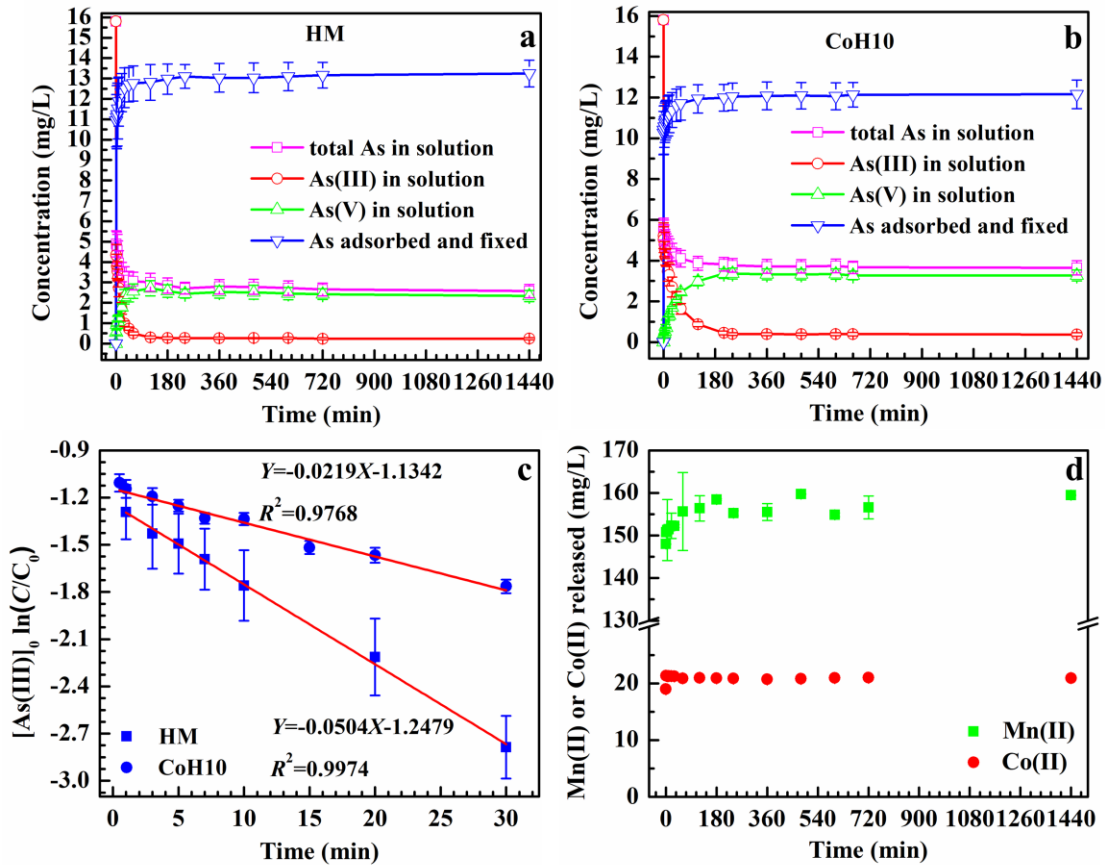
654 As(V) concentration of 7.5 mg/L and sorbent dose of 1 g/L at 25°C. (b) Adsorption

655 isotherm curves of As(V) on Co-doped hausmannite samples, overlaid with the best fit

656 using the Freundlich model,  $Q = kC^{1/n}$ , where  $Q$  is the amount of adsorbed As(V),  $C$  is657 the equilibrium concentration,  $K$  is the distribution coefficient, and  $n$  is a correction

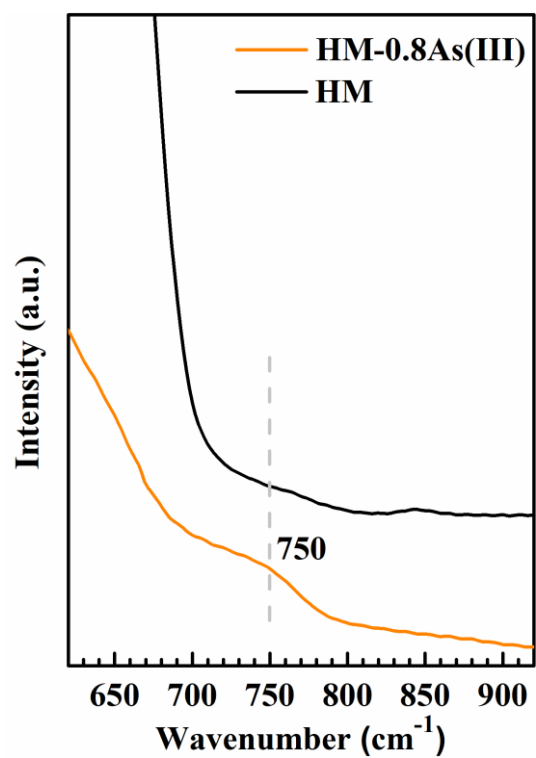
658 factor. Experimental conditions: a sorbent dose of 1g/L, ionic strength of 0.1 mol/L,

659 and a pH of 4.5 at 25°C.



660

661 **Fig. 2** Changes in the concentrations of various As species in solution and on the solid  
 662 surfaces with time during the oxidation of As(III) by HM (a) and CoH10 (b), and (c)  
 663 pseudo-first order kinetic modeling for As(III) depletion by HM and CoH10 at pH 4.5  
 664 during the first 30 min, and (d) release of Mn(II) or Co(II) during the As(III) oxidation  
 665 by CoH10. Experimental conditions: mineral concentration = 0.5 g/L,  $[\text{As(III)}]_0 = 15.8$   
 666 mg/L and  $[\text{NaNO}_3] = 0.1$  mol/L.



667

668 **Fig. 3** FTIR spectra of pristine HM and that after reaction with As(III).

669

670

671

672

673

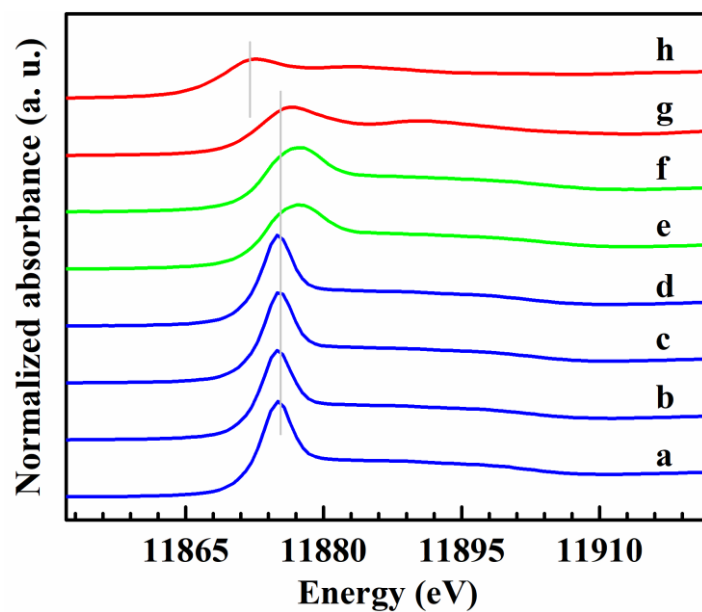
674

675

676

677

678



679

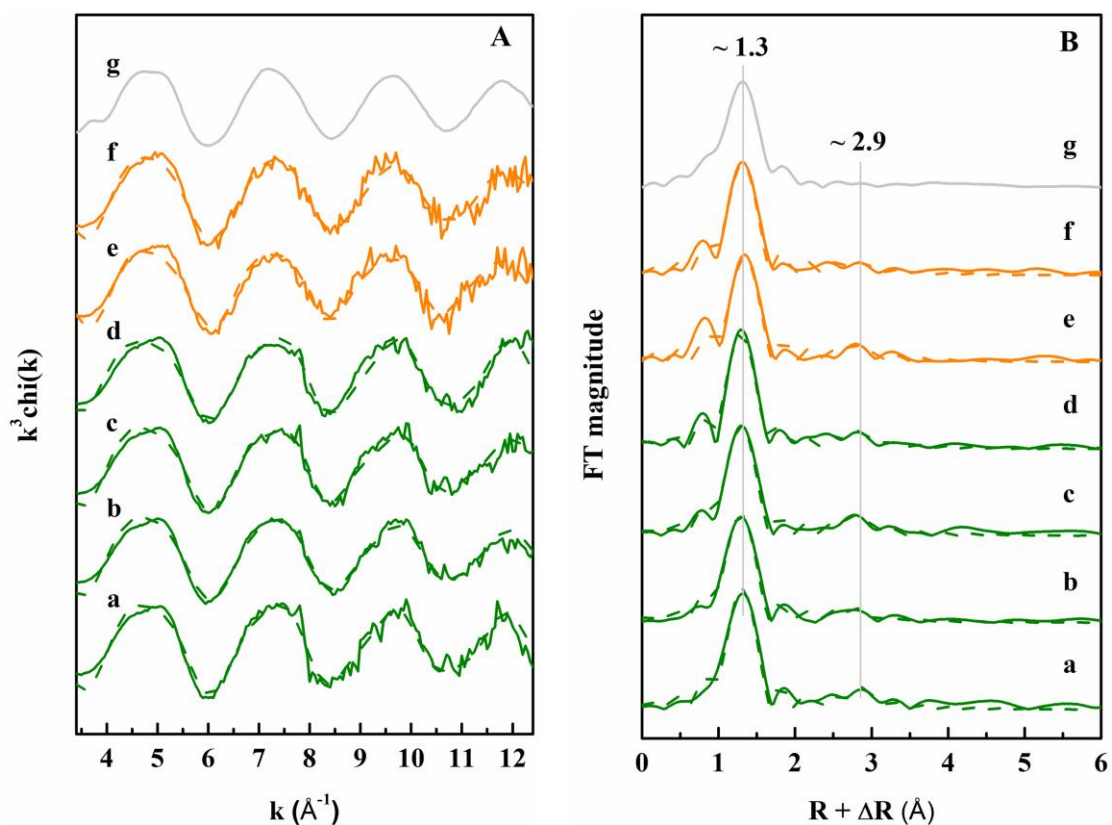
680 **Fig. 4** Normalized As K-edge XANES spectra of reference samples ( $\text{As}_2\text{O}_3$  and  
 681  $\text{Na}_3\text{AsO}_4$ ), and HM and CoH10 after As(V) adsorption ( $[\text{As(V)}]_0 = 0.05$  and  $0.40$   
 682 mmol/L) and As(III) oxidation ( $[\text{As(III)}]_0 = 0.8$  mmol/L). (a) HM\_0.05As(V), (b)  
 683 HM\_0.40As(V), (c) CoH10\_0.05As(V), (d) CoH10\_0.40As(V), (e) HM\_0.80As(III),  
 684 (f) CoH10\_0.80As(III), (g)  $\text{Na}_3\text{AsO}_4$  and (h)  $\text{As}_2\text{O}_3$ .

685

686

687

688



689

690 **Fig. 5** (A) As K-edge EXAFS and (B) the corresponding Fourier transformed spectra  
 691 (FTs) of HM and CoH10 after As(V) adsorption ( $[\text{As(V)}]_0 = 0.05$  and  $0.4$  mmol/L) and  
 692 As(III) oxidation ( $[\text{As(III)}]_0 = 0.8$  mmol/L). The lines are experimental data, and dashed  
 693 lines are the best fits.

694 (a) HM\_0.05As(V), (b) HM\_0.4As(V), (c) CoH10\_0.05As(V), (d) CoH10\_0.4As(V),

695 (e) HM\_0.8As(III), (f) CoH10\_0.8As(III) and (g)  $\text{Na}_3\text{AsO}_4$

Effects of cobalt doping on the reactivity of hausmannite for As(III)  
oxidation and As(V) adsorption

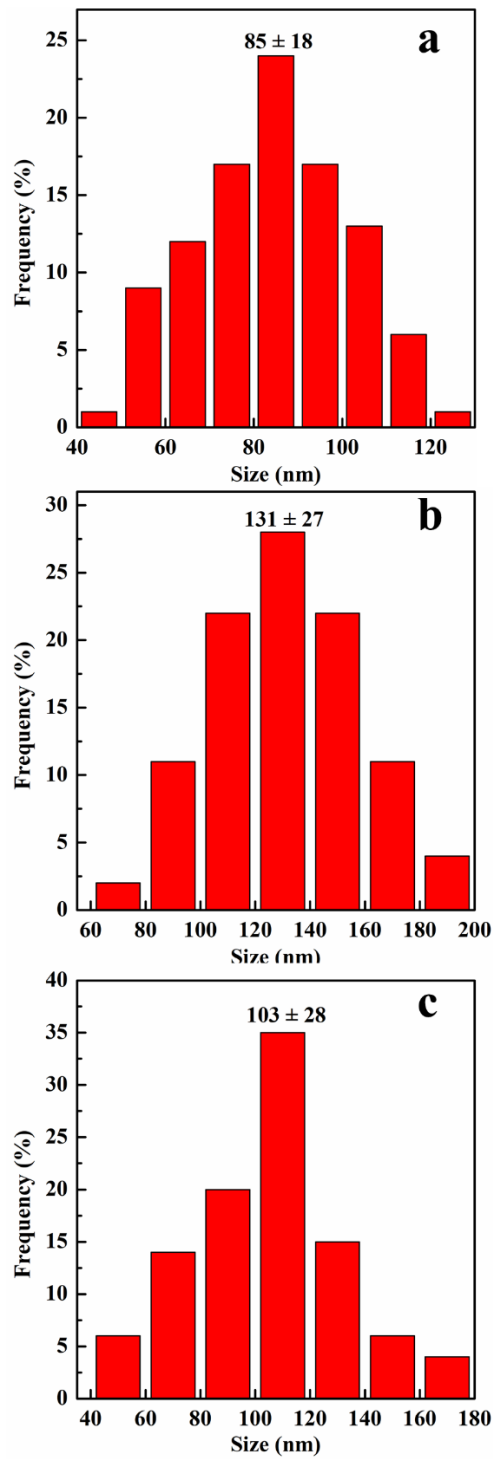


**Fig. S1** Size distribution histograms of Co-doped hausmannite crystals. (a) HM, (b) CoH5, and (a) CoH10. The particle size is a statically average value by analyzing 100 crystals for each sample.

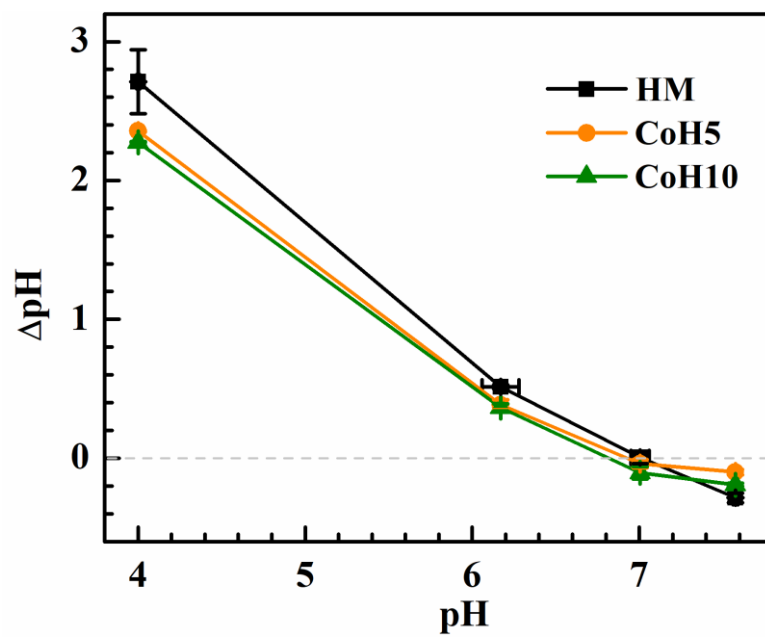


**Fig. S2** The point of zero charge of Co-doped hausmannite samples.

**Table S1.** Fitting results of the isothermal curves for As(V) adsorption onto Co-doped hausmannite samples.

Sample	Langmuir			Freundlich		
	$Q_e$ /(mg/g)	b/(L/mg)	$R^2$	k	1/n	$R^2$
HM	9.55	0.34	0.86	3.88	0.24	0.99
CoH5	7.60	0.62	0.77	3.49	0.23	0.98
CoH10	5.82	0.33	0.85	2.48	0.22	0.91

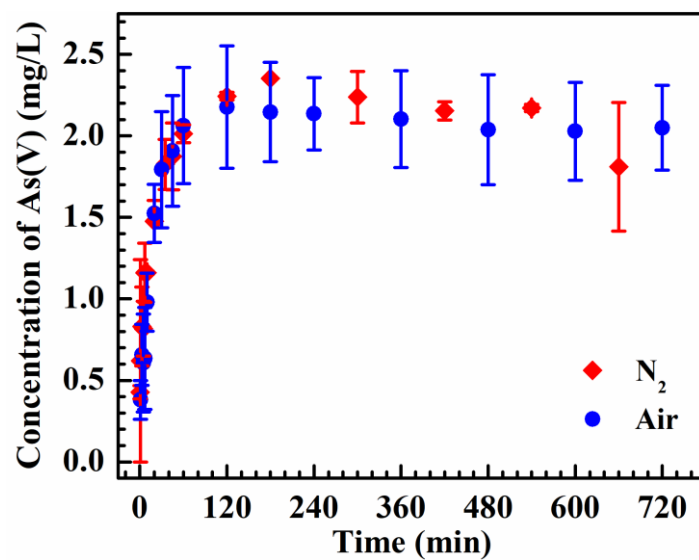


**Fig. S3** Concentration of As(V) in solution during As(III) oxidation by HM under N<sub>2</sub> or air condition. Experiment conditions: pH=4.5, initial As(III) concentration = 15 mg/L, sorbent dose = 0.5 g/L, and ionic strength = 0.1 M NaNO<sub>3</sub> solution.